AN INSIGHT INTO THE FINITE ELEMENT MODELING METHODOLOGY OF: SOIL STRUCTURE INTERACTION ANALYSIS OF DEEP FOUNDATIONS

Dr. Eng. Özgür BEZGİN

İSTANBUL
January 2010

TABLE OF CONTENTS

DEVELOPMENT OF THE FINITE ELEMENT MODEL

1.1 Introduction

In order to create valid model to represent a shaft-soil system, the nature of the soil-structure interaction (SSI) has to be carefully evaluated. The developed model should include all the parameters that influence the lateral response of the soil-shaft system. In addition, the physical characteristics of the system should be defined. The physical characteristics cover a wide range that includes:

- Geometric domain.
- Physical properties of the modeled elements.
- Interactions between the elements.
- Loading and support conditions.
- Possible geometric or physical imperfections.

Two FE models were created for evaluating drilled shaft response due to lateral loads. These models are a 3D continuum model and simplified shaft-spring model based on the Winkler beam theory. Both models will be discussed in detail in this chapter.

1.1.1 Geometric Domain

1.1.1.1 Soil Selfweight Deformations Excluded

The first step to create a SSI model is to define the geometric domain of the SSI system so that the physical interactions can be defined within this domain. Although the radial extension of the soil around the shaft can be considered infinite compared to shaft dimensions, the effective soil zone (E) that participates in the soil resistance

around the shaft is finite as shown in figure 1.1. Therefore the effective soil that needs to be considered within the SSI model should be defined and properly modeled.

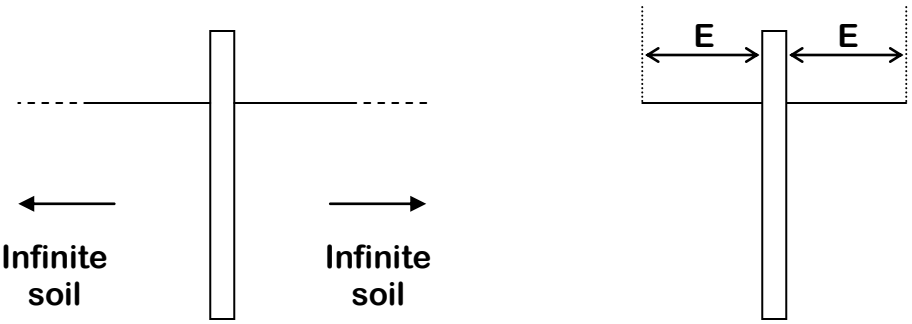

Figure 1.1 – Infinite soil extension and finite representation through modeling.

The model developed to represent SSI includes two elements: 1) Drilled shaft and 2) Surrounding soil. These two elements interact with each other thorough an interface that includes shaft and soil surfaces where normal and shear forces are transferred. The physical domain of SSI includes a bounded drilled shaft and an unbounded soil medium. The drilled shaft has a defined geometry, which can be easily implemented within the model. However, the extent of soil that needs to be included within the model requires an approximate representation.

The lateral load capacity of a shaft-foundation results from:

- The bending behavior of the shaft.
- Load-displacement characteristics of the soil (p-y curves).

Secondary effects due to interface friction, Poisson's ratio, soil shear coupling, and soil confinement.

The bending behavior of the shaft is defined by:

- Elastic modulus
- Moment of inertia
- Support conditions

The elastic modulus and the moment of inertia of the shaft are independent from the surrounding soil. However, the boundary conditions of the shaft are dependent on the soil. Although the drilled shaft usually has some type of support at the base, it will be assumed for now that the shaft is supported by soil only i.e. there is no rock socket. Therefore the only radial and longitudinal support comes from the soil. Under a lateral load, the shaft will deflect causing a curvature along the shaft thus creating resistance due to bending as shown in figure 1.2. The primary role of the soil in lateral resistance of the shaft is that the soil acts as a continuous and variable support along the shaft depth that is critical for determining the shaft curvature.

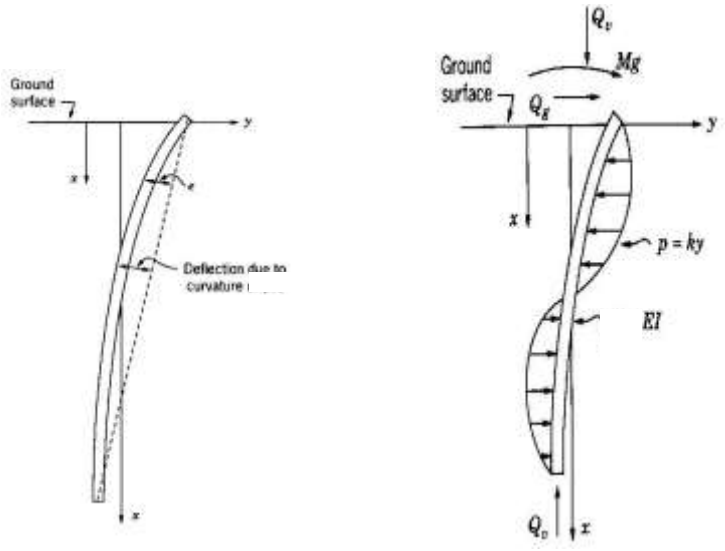

Figure 1.2 – Shaft deflections and curvatures under lateral loads.

The soil stiffness and the shaft stiffness are the two factors that affect the curvature of the shaft and define the lateral strength of the soil-shaft system.

The curvature of the shaft under same loading conditions but in different soil media with different strength parameters will also be different. Thus the curvature of the shaft is a result of the interaction between the soil and shaft, which is based on their

relative stiffness. The effective extent of the soil that should be included in the model will be evaluated through a series of models with varying soil extensions.

1.1.1.2 Soil Selfweight Deformations Included

The other factor that influences the soil-structure behavior is the soil selfweight deformations. The confining effects of the soil due to its self-weight have rarely been evaluated in SSI models. Figure 1.3(a) and figure 1.3(b) show the plan and profile distribution of the confining pressure around the shaft.

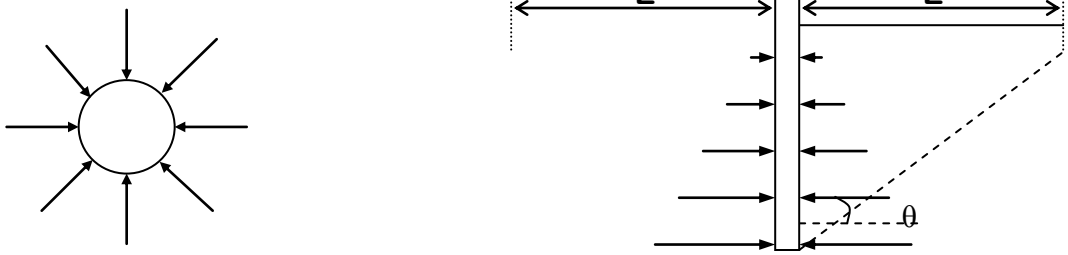

a) Cross-section of the shaft and the radial soil pressure.

b) Finite soil representation.

Figure 1.3 – Confining pressure due to soil selfweight deformations.

The soil behavior in its unsupported state is much like in the case of a soil retained by a retaining wall, where the soil mass behind the wall is within the danger of partial collapse under its own weight without the wall. Soil can be considered as a continuum and the stress distribution is very much dependent on the state of neighboring regions within this continuum. If the structural continuity is disturbed in any way within this continuum, the state of stress within could lead to a state of imbalance because every unit of soil is a support to the neighboring soil units. The shear strength of a soil mass is the resistance per unit area against sliding along internal

planes. Figure 1.4(a) shows the biaxial state of stress of a unit volume of soil element under its own weight and figure 1.4(b) shows the Mohr-Coulomb failure criteria.

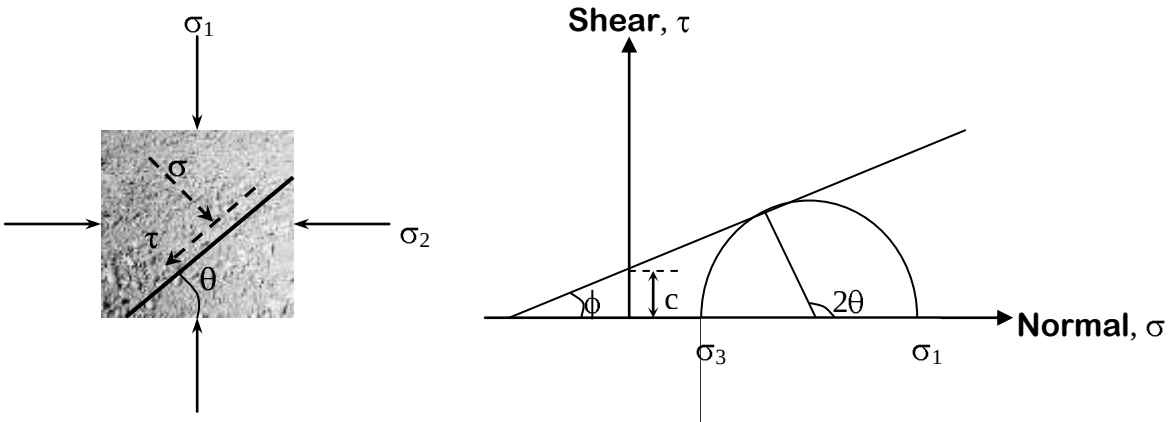

a) Inclination of failure plane.

b) Mohr's circle and failure envelope.

Figure 1.4 – Biaxial state of stress and Mohr-Coulomb failure criteria for soil.

Under the influence of stresses caused by the soil selfweight σ_1 and the resulting horizontal stress σ_2 which is related to the vertical stress through $\sigma_2=K_0$. σ_1, the resulting state of stress in a plane at some point within the soil is such that the shear stress within the plane is equal to the resisting friction force that is created by the normal stress within the plane. The shear strength τ is given by:

$$\tau = c + \sigma\tan\varphi \qquad (1)$$

Where ϕ is the angle of internal friction, c is the cohesion, and $\tan\phi$ is the friction constant of the soil. When the horizontal stresses are overcome by the vertical stresses due to selfweight, collapse occurs. Retaining walls are built to provide the strength needed to achieve the necessary lateral stresses within the soil. In the case of soil continuum the neighboring soil units mutually provide this extra strength. Thus if a hole is drilled in the soil, the lateral support is lost and collapse may occur.

The critical plane where the sliding can occur makes an angle θ with the horizontal that can be related to ϕ through:

$$\theta = 45 + \varphi/2 \qquad (2)$$

The soil volume that should be included in the model where the soil selfweight deformations and the resulting confining stresses are effective depends on ϕ which is a property of the soil. From figure 1.3(b) it is seen that the effective soil volume for confinement is related to the critical plane inclination according to the following relationship, where L is the depth of the shaft:

$$E = L\cos\theta = L\cos(45+\phi/2) \qquad (3)$$

The mass of soil above this plane has the potential to slide and confine the drilled shaft, thus the soil volume that extends an amount E radially should provide the necessary domain to analyze the effect of selfweight deformations.

This effective soil volume will be validated through various models with different soil extensions.

1.1.2 Properties of the Modeled Elements

The SSI model includes two elements: the shaft and the soil. The drilled shaft is made of concrete. The concrete in the drilled shaft is standard Type-I Portland Cement, sand and gravel concrete with the following properties based on ACI code evaluations:

$f_c^{'} = 4000\,\text{psi}$

$f_t^{'} = 7.5\sqrt{f_c^{'}} = 474\text{psi}$

$w_c = 145\text{pcf}$

$v = 0.25$

$E_c = 33 w_c^{1.5}\sqrt{f_c^{'}} = 57000\sqrt{f_c^{'}} \cong 3.600.000\text{psi}$

The concrete stress strain behavior is shown in figure 1.5 where the linear-elastic behavior terminates at a strain level of 0.0005 after which the strain-hardening region remains linear until compressive failure at a strain level of 0.003. Under tension the response remains linear until at a strain level of 0.0001 at which rupture occurs.

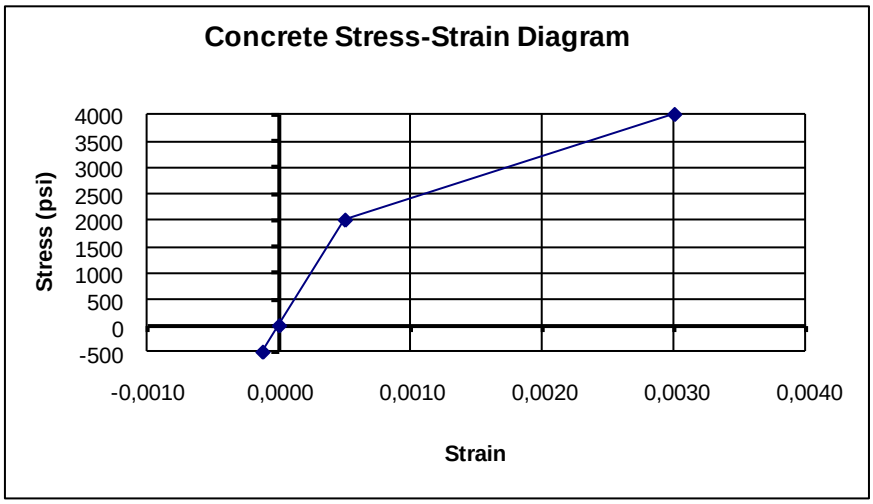

Figure 1.5 – Stress-strain variation of normal weight fc'=4000 psi concrete.

The soil used in the FE model is dry-sand. The relevant parameters of the sand are highly variable due to their dependence on its void ratio, and particle characteristics such as roundness and angularity.

The void ratio, e, of soil is used to characterize the level of compactness of the soil. It is defined as:

$$e = V_v / V_s \qquad (4)$$

Where V_v= volume of voids within a unit volume of soil

V_s= volume of solid within a unit volume of soil

The unit weight, internal angle of friction, and the coefficient of subgrade modulus are dependent on these characteristics. The unit weight of the soil could vary between 100 pcf for loose sand with void ratio e=0.8 to 130 pcf for dense sand with e=0.45.

Also angular sands tend to have a higher unit weight than round sands due to lower void ratios because they can achieve a much better compactness compared to round grained sands.

The friction angle is dependent on particle geometry and void ratios as well. Table 3.1 provides friction angle values for sand with different composition.

Table 1.1 – Variation of friction angle with soil type and compactness (Das, 1998)

Soil Type	Φ (deg)	e
Sand: Rounded grains		
Loose	27-30	0.8
Medium	30-35	0.6
Dense	35-38	0.4
Sand: Angular grains		
Loose	30-35	0.8
Medium	35-40	0.6
Dense	40-45	0.4

The majority of the FE models for cohesionless soil evaluated in this study were for dense dry sand with the following properties:

$w_s = 125 lb/ft^3$
$v = 0.3$
$\varphi = 36^\circ$
$n_h = 50 lb/in^3 = 86.4 kip/ft^3$

The elastic modulus of the soil was assumed to vary linearly with depth and the value of the rate of change in modulus with depth (i.e. coefficient of subgrade modulus) was selected from the diagram shown in figure 1.6.

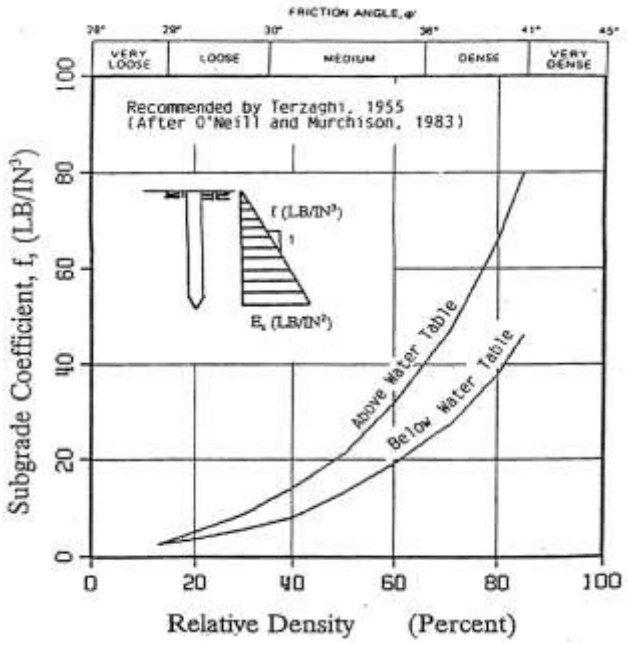

Figure 1.6 – Subgrade coefficient versus density for sand (Terzaghi, 1955)

The stress-strain characteristics of the soil along the shaft depth were modeled as elastic-perfectly plastic. The yield strain of the soil at a certain depth was calculated based on the yield displacement following the API procedure (1993). The ratio of the elastic displacement at a certain depth to the effective soil volume was used as the yield strain at a specific depth. As it will be shown later in this chapter, the effective soil volume extends about 2.5D away from the shaft surface (Type-1 FEM).

This procedure was applied to medium-dense sand used in the FE models with the following properties:

$K_o = 0.4, K_A = 0.26$

The 100 ft sand profile was discretized into 2.5 ft layers and the steps outlined for the API procedure were applied resulting in the parameters tabulated in table 1 and 2 in the Appendix, which were then used to obtain the p-y curves, which are tabulated in figure 1, 2 and 4 in Appendix. Typical p-y curve is shown in figure 1.7.

The bulk of the lateral resistance of a deep foundation comes from the top layers of the soil, which extends about 5 to 6 shaft diameters below the ground. The API procedure provides non-linear p-y curves for the upper layers within this effective depth. For deeper layers the API procedure presents only the linear portion of these curves.

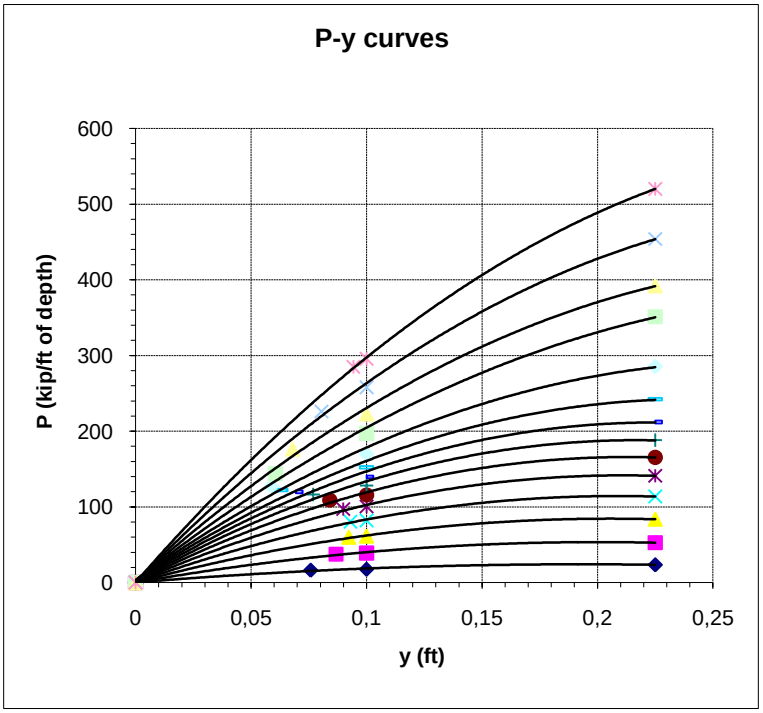

Figure 1.7 – P-y curves for the 100ft deep 6 ft diameter shaft in dense sand.

The Drucker-Prager failure criterion was used in the FEM because the strength increase due to pressure and the intermediate principal stresses are accounted for in these criteria.

1.1.3 Modeling Surface Interaction Between the Soil and the Shaft

The interaction between the shaft and soil elements within the SSI involves the transfer of contact pressure and shear stresses due to friction between the interacting surfaces. The interacting surfaces are the boundary surface of the shaft,

and the interior surface of the soil in contact with the shaft. The contact pressure is related to formation of gaps between the surfaces. The presence of a gap between the two surfaces indicates that there is no transfer of normal stresses or the pressure is zero. The closure of a gap enables the formation of a contact pressure. If g denotes the gap width, then the following representation regarding the pressure between the surfaces could be made:

$$p = \begin{Bmatrix} p(x) & \text{when } g = 0 \\ 0 & \text{when } g > 0 \end{Bmatrix} \quad (5)$$

Where p=p(x) represents the dependence of the pressure to the surface deformation which is denoted by x. The case where g < 0 is non-existent as this would represent the surfaces moving through each other.

Another interaction that is included within the SSI is related to the friction that exists between the surfaces. In most SSI models the friction forces generated at the interface are overlooked. Figure 1.8 shows the drag forces that are generated due to surface friction whose value is dependent on the pressure and the coefficient of dynamic friction of the interface. These drag forces provide additional strength to the overall lateral resistance provided by the soil. The shear stresses due to drag forces can be related to the pressure at the interface as follows:

$$\tau_d = p.\mu_k \quad (6)$$

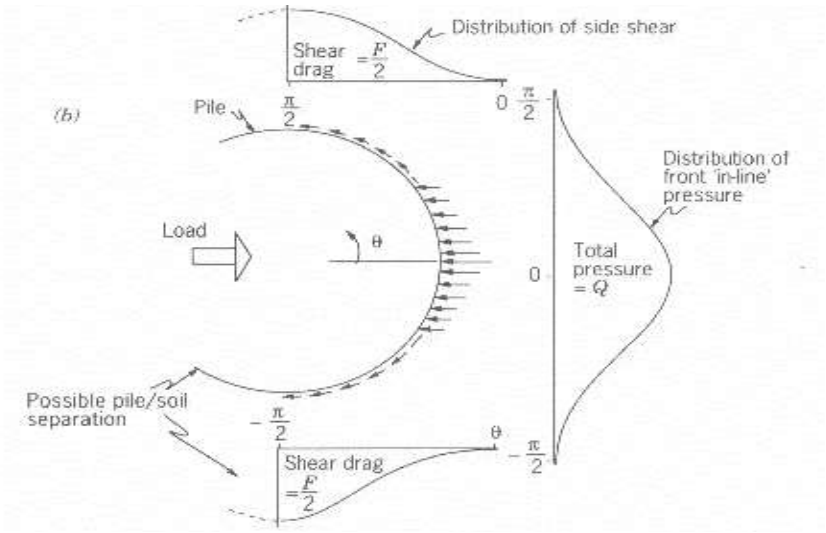

Figure 1.8 – Cross-section of a shaft showing the shear stresses due to friction (Smith,1987)

The drag forces could be related to the motion of the shaft through the signum function, which simply relates the drag force to motion. Figure 1.9 shows the shear stresses generated due to friction. The shear stresses can be related to the motion through:

$$\tau = \tau_d \text{sign}\left(\dot{x}\right) \quad \text{where} \quad \text{sign}\left(\dot{x}\right) = \begin{cases} -1 & \text{when} \quad \dot{x} < 0 \\ 0 & \text{when} \quad \dot{x} = 0 \\ +1 & \text{when} \quad \dot{x} > 0 \end{cases} \tag{7}$$

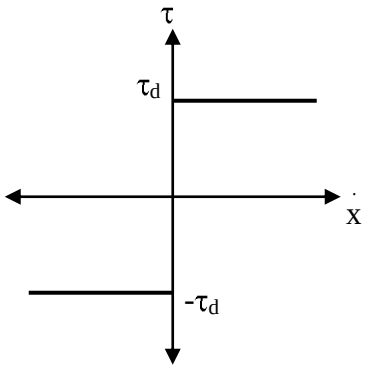

Figure 1.9 – Shear stresses at the interface due to friction and direction of motion.

1.1.4 Loading and Support Conditions

The response of any structure is affected by the loading on the structure and its support conditions as well as its physical conditions and interactions with surrounding structures. A support modifies the mobility of a structure to a certain specified degree thus modifying the global response of the structure through the modification of its curvature. Motion of a structure can be characterized in terms of translation and rotation. Partial or full prevention of one or the other or both of these motions results in a different structural response under loading. An exact assessment of support conditions is difficult and a certain level of approximation is likely to be involved whenever a structure is being analyzed. There are many reasons for approximating support conditions. These include: 1) lack of data, 2) complexity of details and 3) lack of analytical methods to idealize support conditions. When a structure is characterized as fixed supported; it is assumed that the structure is fully restrained in terms of translation and rotation at the support location. It is possible that partial rotation and translation could exist at the support. Shafts that have rock sockets are assumed to be fully fixed at the bottom. However, shafts that rest on a stiff layer of soil surface or shafts that partially penetrate into a stiff layer of soil may not be considered as fully fixed at the bottom. Figure 1.10 represents the reaction forces on a laterally loaded shaft that rests on stiff soil. The bottom of the shaft that rests on the stiff soil is also enlarged to show the displaced shape and the reaction forces before and after the loading.

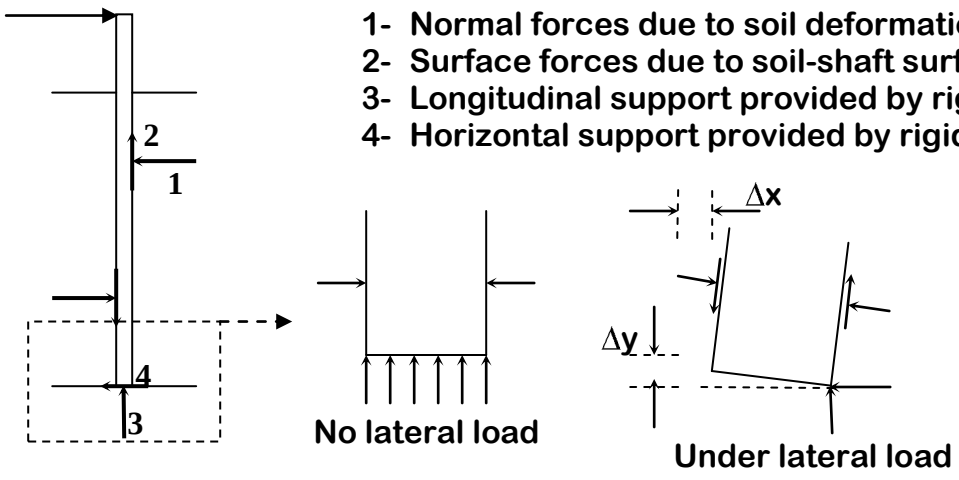

Figure 1.10 – Reaction forces on a laterally loaded shaft.

Shafts that are not anchored to a rigid layer can translate (Δx, Δy) and rotate θ under the influence of a lateral load as shown in the enlarged view of the shaft base in figure 1.10. The only support provided by the rigid layer is normal support before the loading, and a combination of frictional and normal support after the loading.

In order to model the effect of support conditions on shaft behavior, a FE model has been developed where the soil continuity was extended under the shaft as well. The soil was extended below the shaft a distance equal to twice the shaft diameter. Such an extension allows modeling the rigid layer beneath the shaft and the interactions between the bottom shaft surface and the soil. The support conditions do not have an effect on the shaft response for slender shafts. However, below a certain slenderness value, the support conditions begin to affect the results obtained. Thus correct modeling of the support is necessary for certain values of slenderness.

1.1.5 Effect of Disturbed Soil Adjacent to the Shaft

During the construction of drilled shafts, disturbance of adjacent soil can alter the physical characteristic of the soil. The disturbance produced by the drilling

equipment can alter the elastic modulus of the soil close to the shaft surface that can eventually affect the lateral load capacity of the drilled shaft. Figure 1.11 shows the cross section of a shaft and surrounding soil. The central small diameter circle represents the shaft and the intended diameter of the hole. The gray area around the shaft represents the weak-layer, and the larger dashed circle represents the soil further away from the shaft.

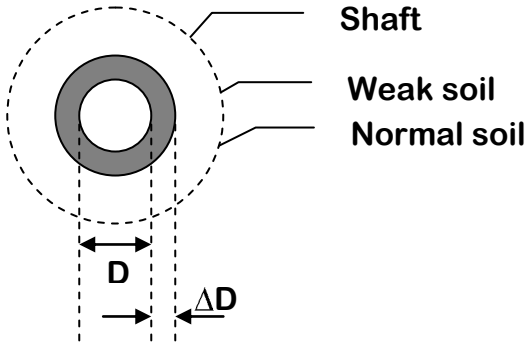

Figure 1.11 – Weak soil adjacent to interface.

Another problem associated with construction techniques could involve the shaft itself where there is a problem with the straightness of the shaft or a continuity problem related to interrupted pouring. The vertical problems are associated with faulty drilling where the hole is not a perfect perpendicular position with respect to the ground level. The problems relating to concrete are most related to interruptions in concrete pouring. Usually the concrete has to be poured at a certain rate in a single uninterrupted pour until the completion of the shaft in order to provide the homogeneity along the length of the shaft. Failure to comply with the rate of pouring could result in slurry, air or groundwater to be trapped within the shaft creating a weak zone along the cross section of the shaft.

One of the advantages of using FE continuum model is that any post-construction structural change can be implemented within the model to see its effect on the design strength of the structure. To this end the soil and shaft meshing will be such that, any weak layer either in soil or shaft can be included

1.2 Modeling of SSI

The FE method was utilized to develop models to represent the SSI for laterally loaded drilled shafts. Different FEM with varying degrees of complexity can be generated to partially or fully represent the SSI characteristics. Complexity or simplicity of a model reflects the degree of approximation the model makes with respect to the behavior of the real structure. Two different finite element models have been configured for comparison purposes:

- Spring model.
- Continuum model.

The finite element program used to develop the models is ABAQUS version 6.4.

1.2.1 Spring Model

The spring model which is based on Winkler spring theory; uses beam elements to model the shaft and spring elements to model the soil along the depth of shaft. The soil stiffness properties are calculated at certain intervals and are represented by springs located at each selected point. The model considers only the load-displacement characteristics of the soil through the use of spring elements, and deformation characteristics of the shaft through the use of beam elements.

Figure 1.12 shows a typical spring model.

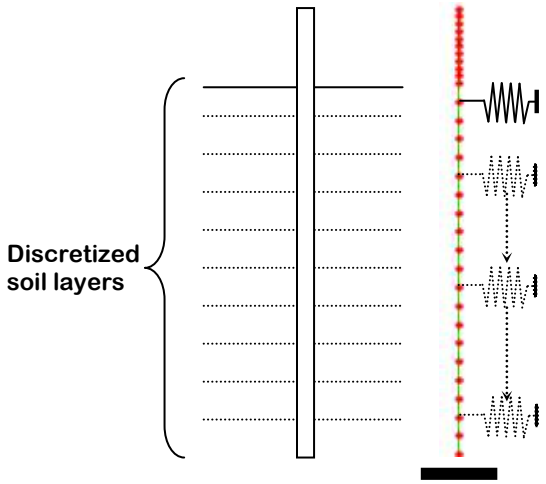

Figure 1.12 – Spring model for a drilled shaft.

The column and the shaft are discretized into nodes along which the physical characteristics such as the cross section and the material properties are defined. The bottom of the shaft is usually supported by a predefined support that has pre-determined characteristics such as roller, pin or fixed. The soil layers are discretized as well and the stiffness properties of each layer is summarized as load-displacement relations and defined by a representative spring. The springs are independent of each other i.e. there is no shear coupling between the springs. The beam elements used are B21 Timoshenko beam elements that consider cross-section deformations due to shear. For slender beams the shear deformations can be disregarded. However, since these models will later be used to model stout SSI models as well, the element selection was conducted to cover all basis. The spring elements are grounded non-linear spring1-type elements. The load-displacement characteristics of the springs are determined through the use of API procedure.

1.2.2 Generation of 3D Finite Element Soil-Shaft Continuum Model

The continuum model makes use of solid elements to define both the shaft and soil within the SSI system, as well as providing interaction between the two through surface definitions. The model considers many structural characteristics of the SSI such as shear coupling within the soil layers, surface friction at the interface, confinement effects due to soil selfweight deformations, and a precise evaluation of the boundary conditions. The generation of the model is not straightforward as the spring model and is highly prone to modeling errors. Therefore the mesh development and optimization is an important first step in generating the continuum model.

1.2.2.1 Mesh Characterization and Element Selection

The first step in development of a FEM is defining the mesh and the selection of elements. It is essential that the mesh properly define the geometry and the effective domain of the system because all the subsequent steps will be defined within this mesh. It is also important that there are no abrupt changes in size within the mesh and the model mesh evolves in a pattern similar to the soil-structure system itself. The character of the mesh reflects the similarities between the mesh generation and the modeled structure. The drilled shaft and the soil are cylindrical elements with a circular cross-section. The meshing for the FEM could be such that the nodes can be defined in a square grid, or they can be described in a radial grid as shown in figure 1.13. A radial characterization of the structure results in a more homogenous mesh and a better characterization of the circular section of the shaft-soil system.

Figure 1.13 – Different approaches to meshing of the SSI model for drilled shafts.

Radial meshing of the cross-section was used at specific intervals along the depth of the shaft, thus creating a 3-D finite element model.

After the mesh generation, the elements were defined. The SSI model is a combination of linear full and reduced integration elements and infinite elements. Since the model also includes surface interactions, the use of linear elements over quadratic elements was preferred due to contact definition difficulties associated with quadratic elements. To this end C3D8 and CIN3D8 elements were used for soil and C3D8R elements were used for the shaft. The choice of reduced integration elements to represent the shaft is to prevent shear locking that occurs in structures subjected to bending loads that are defined by linear full integration elements. One major aspect of the SSI model is the use of finite extension of the soil around the shaft. The determination of the finite effective soil volume around the shaft requires the use of some form of termination method at the soil boundary. This can either be achieved by the use of some nodal support such as rollers, fixed or pinned supports, or by the use of some special form of element that would represent the infinite extension of the soil. Once the effective volume of the soil was determined, full integration linear elements were used to define the soil after which a layer of infinite elements was used.

Table 1.2 – Mesh size per quadrant.

		FEM nodes per quadrant			
	Circle	2	3	4	6
Radius (ft)	3	3	3	3	3
Angle (deg)	-	45	30	22.5	15
# of sectors	-	8	12	16	24
Area (ft^2)	28.27	25.46	27.00	27.55	27.95
% of area		90.0	95.5	97.4	98.9

1.2.2.2 Mesh Optimization

Using radial distribution of nodes that took into account the following criteria resulted in mesh optimization:

- Number of elements per quadrant.
- Transverse discretization of the shaft and soil.
- Longitudinal discretization of the soil layer.

In majority of cases of finite element modeling, using a large number of finite elements leads to more refined results. However, an increase in the number of elements also causes an increase in the execution time, so it is always desired to configure the model with the optimum number of elements. An optimum mesh size is achieved by analyzing a trial design, modifying the mesh, reanalyzing and repeating the cycle until convergence is achieved. The parametric study of the SSI model included variable drilled shaft diameters (D), column heights (H), shaft depths (L), and soil volumes (E). The shaft diameter varied from 6ft to 10ft, the column height from 20ft to 100ft and the shaft depth from 20ft to 100ft. Two models with soil extensions (E) of 2.5D and 8D

were analyzed. These wide ranges of dimensions were chosen to investigate a variety of shaft height-to-depth ratios (L/D).

1.2.2.2.1 Transverse Mesh Density

The FEM for the SSI model being cylindrical in nature, the number of elements to be used per quadrant had to be decided first, since this is a determining factor for the overall number of elements that were going to be in the final model. Such being the case the number of elements were varied from 2 elements per quadrant to 6 elements per quadrant. Displacements and moment were studied for each mesh.

The mesh sizes for the 6ft diameter, 100ft deep shaft with a 20 ft column height loaded with 50 kip lateral load, is shown in table 1.2. As the number of nodes in the model increased, accuracy of the results improved. Figure 1.14 shows the various models with different number of nodes per quadrant.

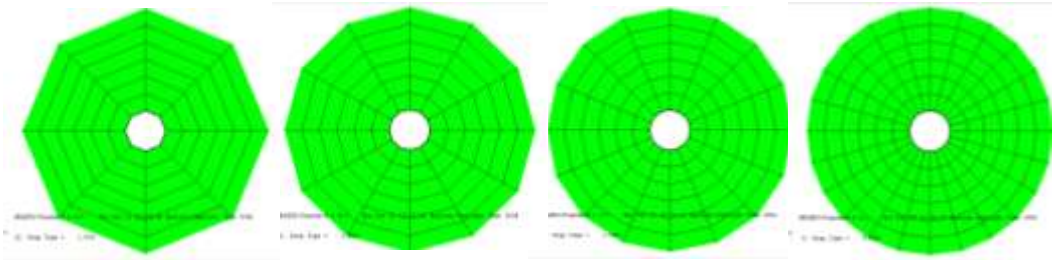

Figure 1.14 – Mesh sizes with varying number of nodes per quadrant.

An increase in the number of elements provides a more refined mesh of the real structure. However, the geometric convergence of the models weren't the only criteria in selecting how many elements per quadrant. To this end, the models were analyzed under the same loading conditions and their response and convergence of displacements, moments and contact pressures was studied. Finally, the decision on the selection of the quadrant divisions was based on this parametric study. The shafts

were loaded with a 50 kip lateral load applied at the top of the column. Displacements, moments and pressures were obtained, and the results were normalized with respect to the results obtained from analyzes with models that included 6 nodes per quadrant. The largest variation in results between these meshes was observed in displacements as shown in figure 1.15. There was difference of about 20% between the results of the 2 nodes per quadrant and 6 nodes per quadrant model. Figure 1.16 shows the variation in moments.

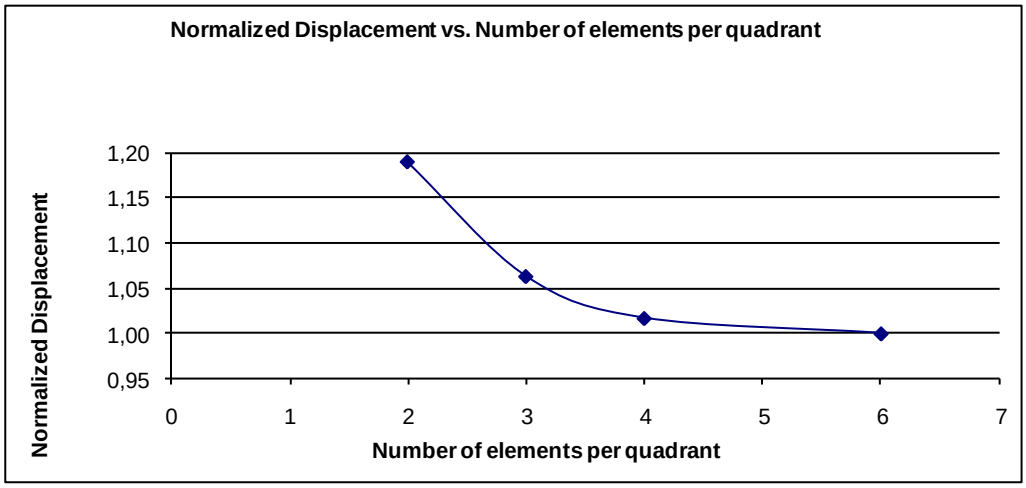

Figure 1.15 - Variation of displacements with number of elements per quadrant.

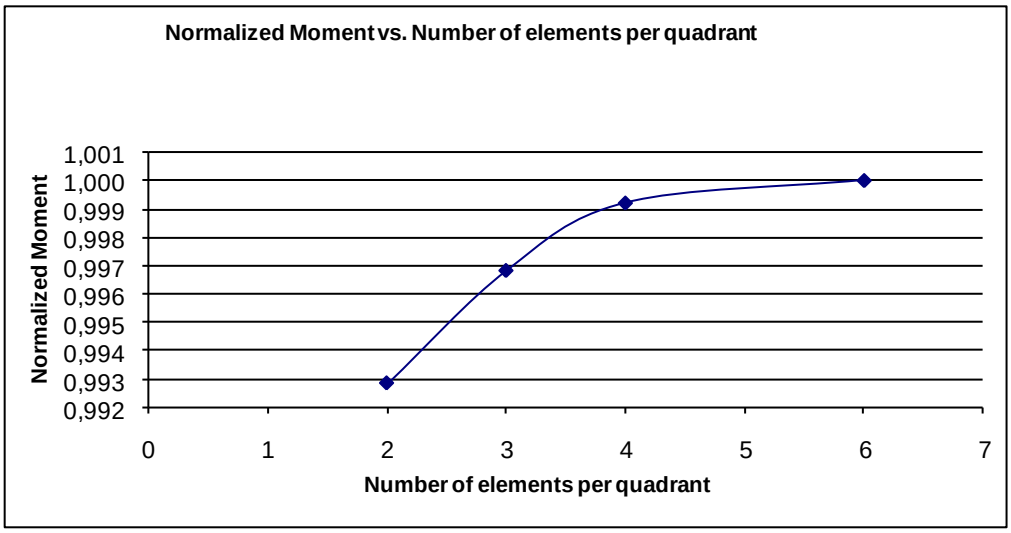

Figure 1.16 – Variation of moments with number of elements per quadrant

The other large variation was observed in rear and front maximum contact pressures, shown in figure 1.17, which was about 13% larger for the 2 nodes per quadrant mesh compared to the 6 nodes per quadrant.

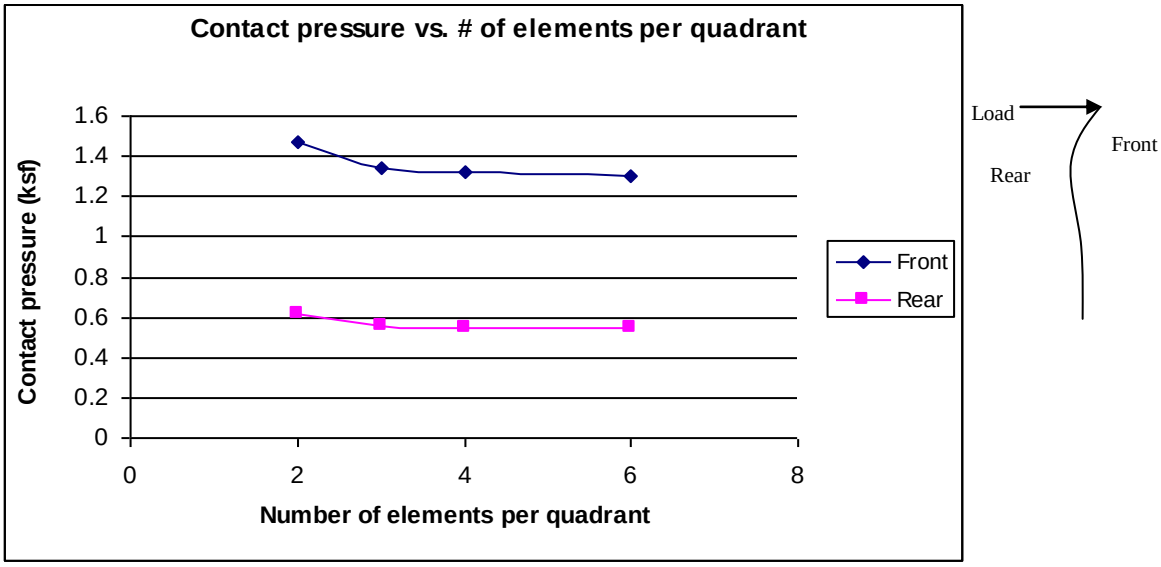

Figure 1.17 – Variation in contact pressure with number of elements per quadrant.

These observed differences in displacement and pressure values are mainly due differences in cross-sectional area represented by the different meshes. The mesh with 2 nodes per quadrant achieved only 90% of the real circular shaft cross section, where the mesh with 6 nodes per quadrant achieved 99%. This difference in area had an effect on displacements and contact pressures but not on moments.

On the other hand, the mesh with 4 nodes per quadrant differed from the 6 nodes per quadrant by approximately 1.5% for displacement and contact pressure. Since this difference was not significant, every layer of soil and shaft elements included 4 nodes per quadrant and a total of 16 elements per layer.

1.2.2.2.2 Longitudinal Mesh Density

FE models for three different shaft lengths 100ft, 50ft, and 20ft with 6ft diameter and 20ft column height were analyzed with different mesh densities along the shaft, ranging from coarse meshes with element sizes 10% of the overall shaft depth to fine meshes with element sizes 2% of the overall shaft depth. The longitudinal division varied from 10% to 2% for the 100ft shaft, 10% to 2.5% for 50ft shaft, and 10% to 5% for 20ft shaft. The three models had depth to diameter ratios (L/D) of 16.7, 8.3 and 3.33 respectively. The analyses of three mesh sizes showed that the shear deformations are not significant for the shaft with high slenderness ratios, but were significant for stout models such as L/D=3.33. As the depth to diameter ratio decreases, the response of the model to lateral loadings was less affected by the longitudinal mesh size. The shafts were fixed at the base and subjected to 50kip load at the top of the column. Figure 1.18 shows a comparison of displacement, moment and shear along the 100ft deep shaft.

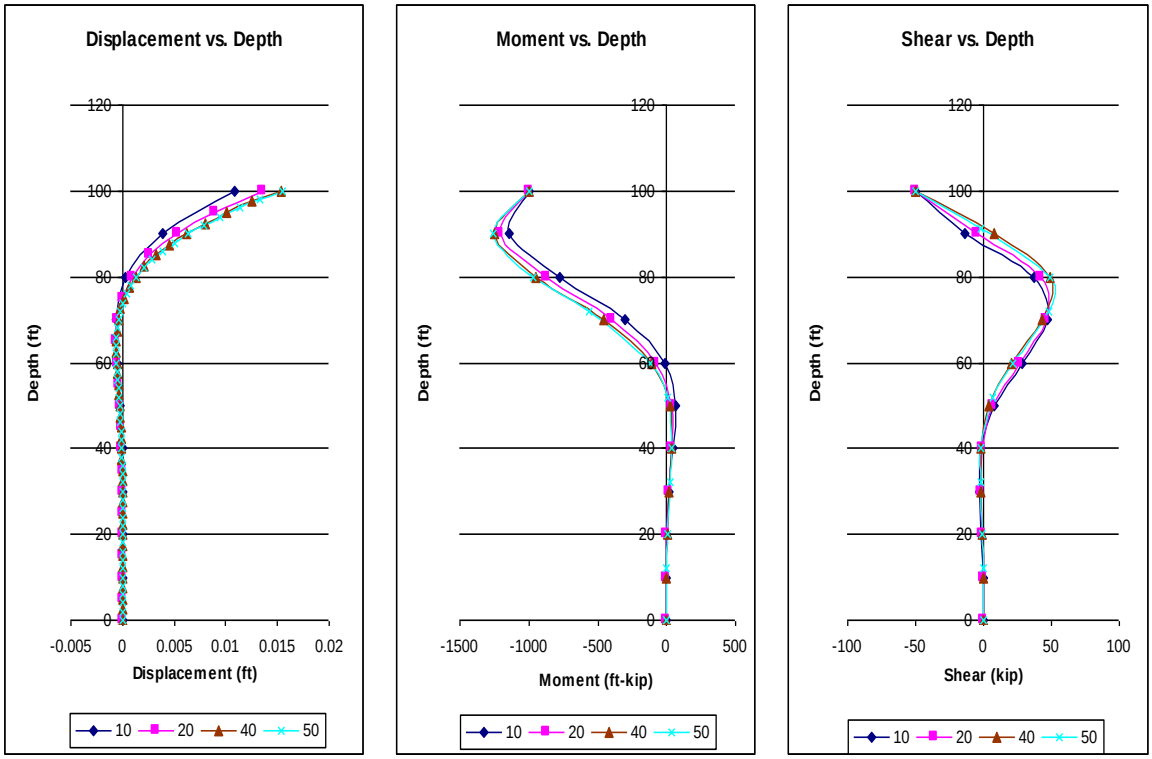

Figure 1.18 – Displacement, moment and shear variations for 100ft deep shaft.

Table 1.3 – Normalized variation for 100ft mesh

	% Difference		
No. of layers	**10**	**20**	**40**
Displacement	29.7	12.7	0.7
Moment	10.7	4.6	0.8
Shear	8.4	7.0	0.9

The reference for the data in table 1.3 was the 2% mesh that included 50 elements along the depth of the shaft. The mesh size also had an effect on the location of the inflection points as shown in figure 1.18. However, the gain from increasing the number of elements longitudinally from 40 to 50 is small compared to the burden that

is placed on the execution time of the model. Thus a 2.5% level of fineness or a 40-layer model was chosen.

Figures 1.19 shows a comparison of displacement, moments, and shears along the shaft for the 50ft shaft. Based on the results of previous analysis of 100ft shaft, the longitudinal mesh included 40 layers. The reference for the data in table 1.4 was the 2.5% mesh that included 40 elements along the depth of the shaft

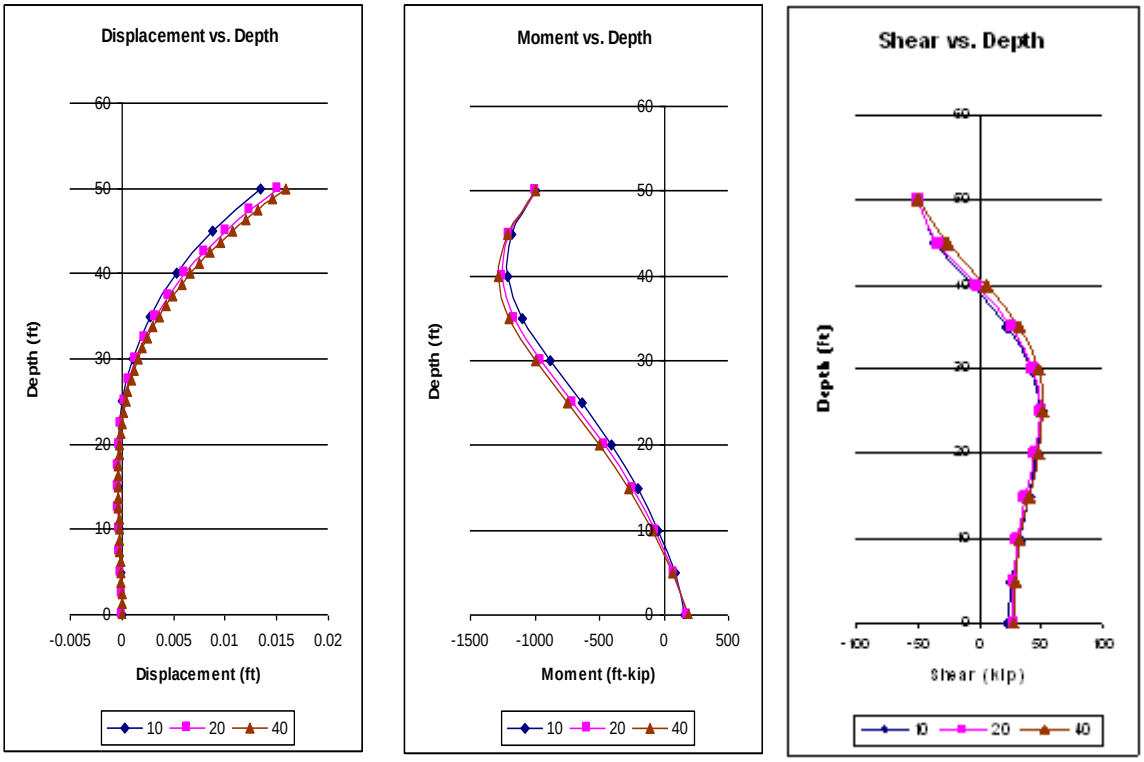

Figure 1.19 – Displacement, moment and shear variations for 50ft deep shaft.

Table 1.4 – Normalized variation for 50ft mesh

	% Difference	
No. of layers	**10**	**20**
Displacement	15.64	5.56
Moment	5.6	2.1
Shear	4.5	1.8

Figure 1.19 shows that as the depth to diameter ratio decreased, number of contraflexure points decreased as well and the location of the inflection point of the moment diagram became lower to the shaft support. Figures 1.20 shows a comparison of displacements, moments and shears for the 20ft shaft. At such a low level of slenderness, the model was virtually un-affected by the level of meshing. The only valid difference was observed in the support shear. Results were tabulated in table 1.5 with respect to 10-layer model. Based on these runs, it was decided that it is sufficient to model the shaft longitudinally at a level at which the element size is 2.5% of the overall length.

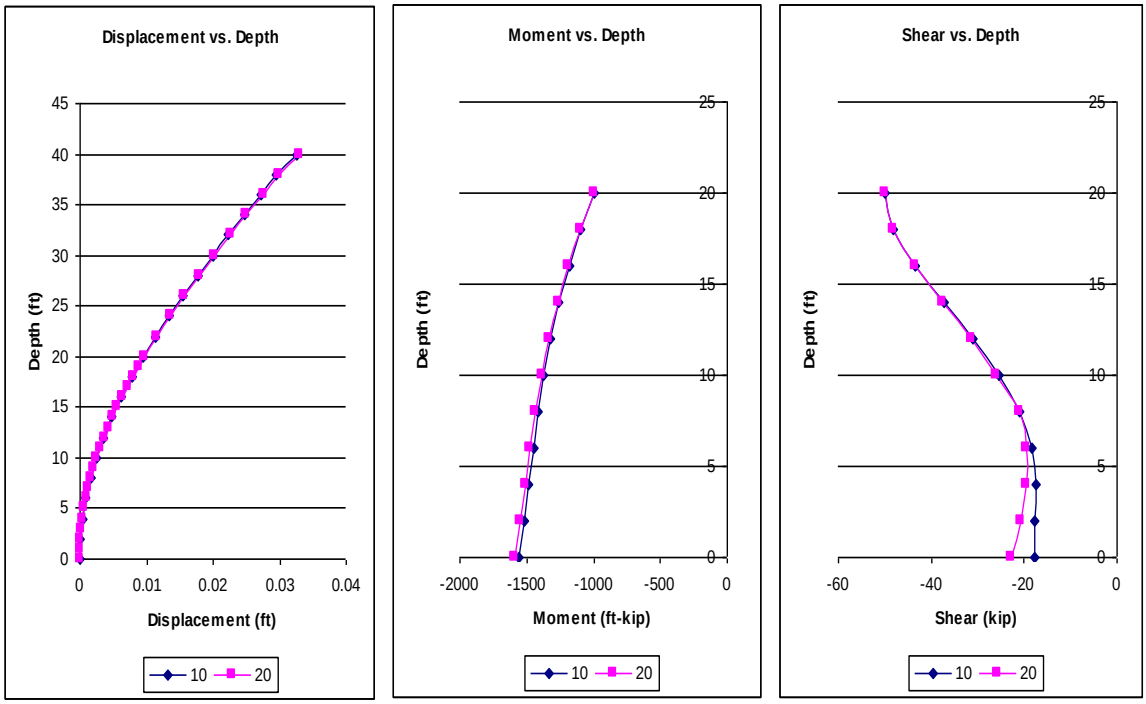

Figure 1.20 – Displacement, moment and shear variations for 20ft deep shaft.

Table 1.5 – Normalized variation for 20ft mesh.

	% Difference
No. of layers	20
Displacement	1.2
Moment	2.1
Support Shear	21.5

1.2.2.2.3 Effective Soil Participation

Following the configuration of transverse and longitudinal distribution of the mesh of the shaft, the soil mesh and mesh density were analyzed. Determination of the amount of soil around the shaft that has effective participation in the shaft response was important in defining the proper SSI model. It was found that the effective soil volume in the transverse direction away from the shaft surface and the amount of layers that had to be used was different based on the inclusion or exclusion of the soil self-weight.

1.2.2.2.3.1 SSI Modeling Excluding Soil Selfweight

The analyzes for an optimum mesh was based on a 6ft diameter, 100 ft deep shaft with a 20ft column height, which resulted in a shaft depth to diameter ratio of 16.7. The results based on this study were applied to other SSI models with different dimensions that resulted in lower depth to diameter ratios. For the FE models that included the lateral stiffness of the soil and not its selfweight (Type-1 FEM), a 2.5D soil extension from the shaft surface with radial distribution of 6 layers of elements was sufficient to capture soil stresses and displacements. The selection of soil extent away from the shaft surface was mainly based on the soil deformations pattern. As

can be seen from figure 1.21 the variations in displacement, moment, and maximum contact pressure beyond 2.5D were not significant.

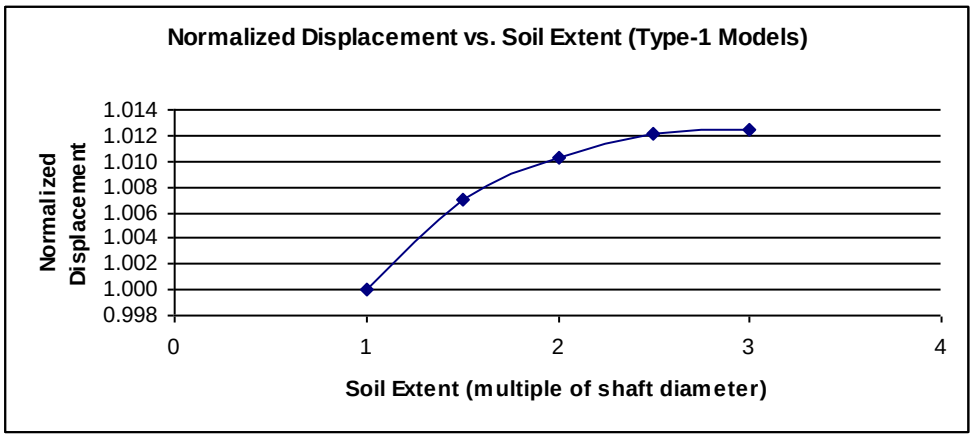

(a)

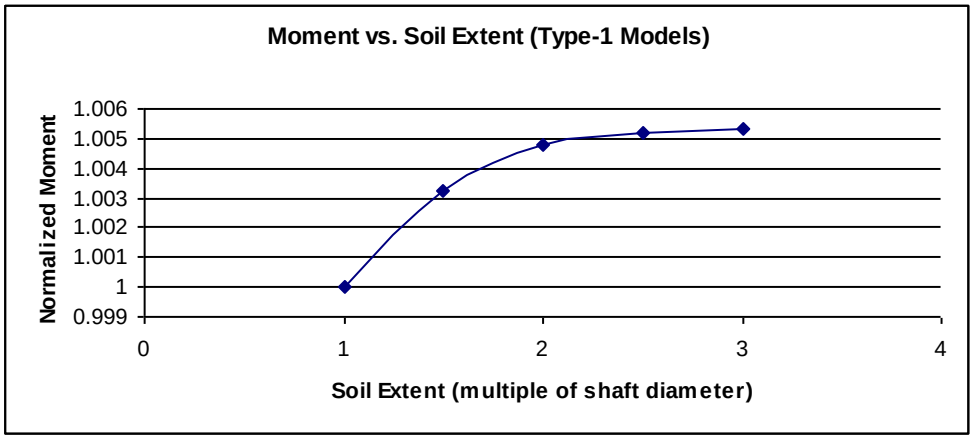

(b)

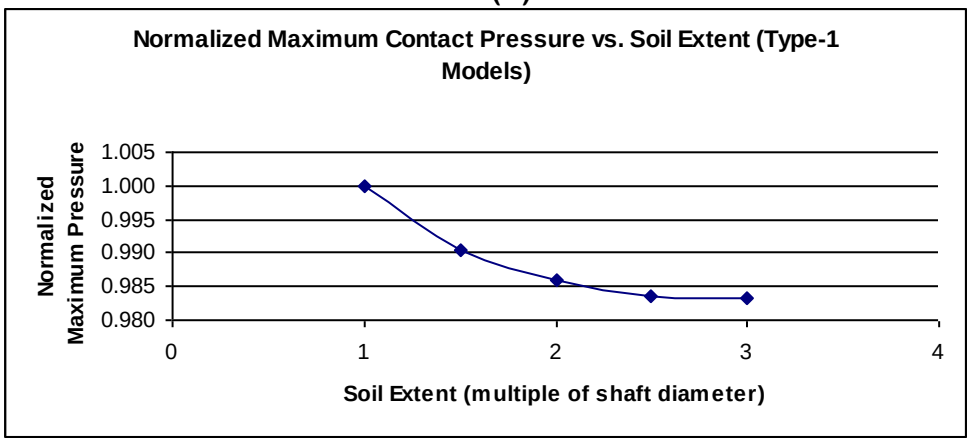

(c)

Figure 1.21 – Variations in (a) displacement (b) moment and (c) maximum contact pressure

The patterns of lateral displacements of the soil are shown in figure 1.22. This figure clearly shows that the 2.5 D soil extension is sufficient to model the soil-structure system in this study. This capability to monitor the full soil deformations in this model enables us to analyze the fixity conditions and effects of poisson's ratio of soil on the shaft behavior as a part of parametric analysis. Therefore the 2.5D model was used throughout the studies where the soil selfweight was not included.

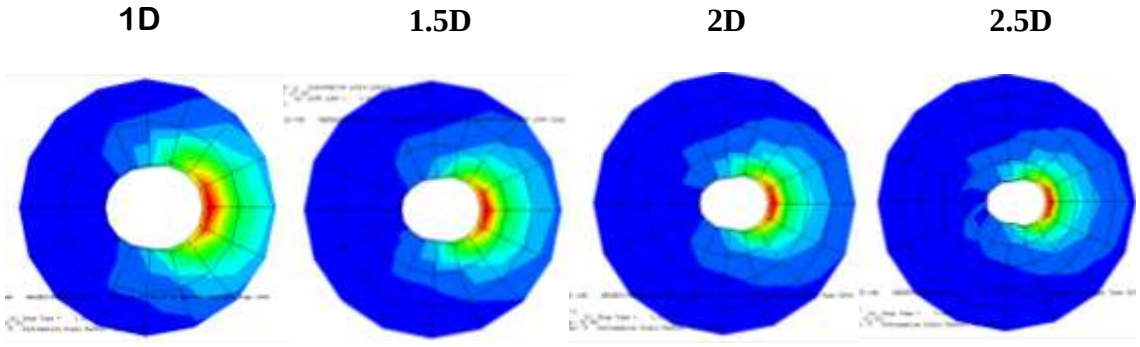

Figure 1.22 – Lateral soil displacements with different soil extensions.

Following the determination of the optimum soil extension, the division of this extension was configured. The 2.5D soil extent was divided in to 2,3,4,5 and 6 layers and analyzed under a 50 kip lateral loading. The division of the soil extent away from the shaft surface and the displacement patterns associated are shown in figure1.23.

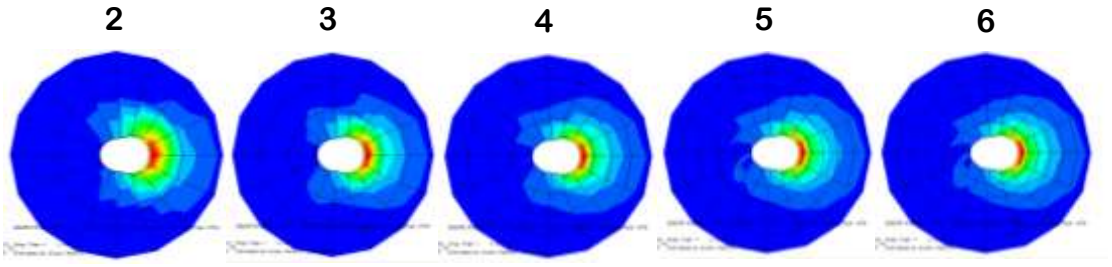

Figure 1.23 – Variation of displacements with different layering.

The soil deformation patterns as well as the displacement values are completely captured in a 6-layer model. The variation of normalized displacements with number of layers is shown in figure 1.24. An increase in layers from 2 to 6 results in an increase in displacement of 3%. Note that the final layer of soil elements is reserved for the infinite elements that represent soil infinite extension in the transverse direction.

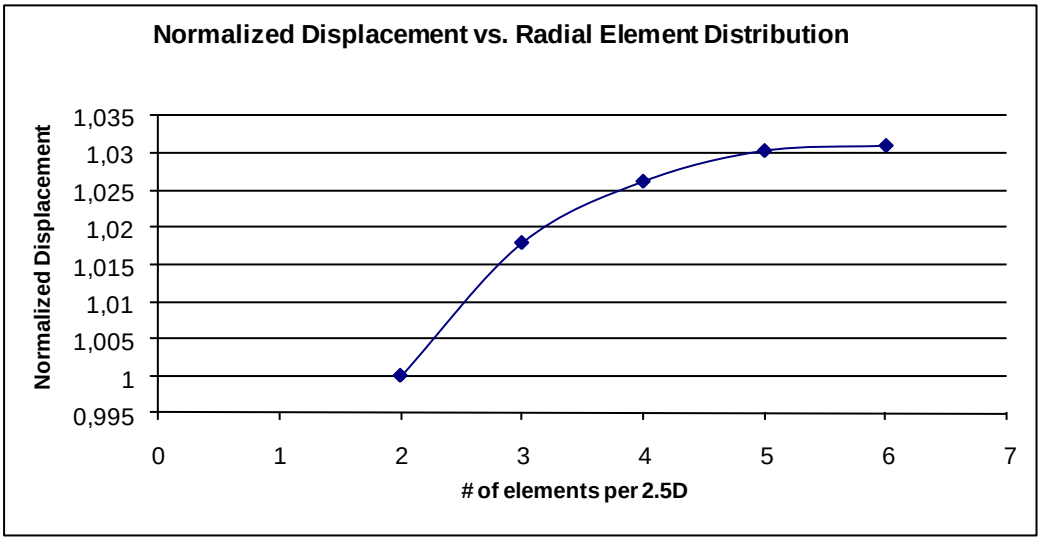

Figure 1.24 – Percentage increase in displacements with increasing number of layers.

The configuration of the transverse and longitudinal division of the mesh has so far been decided based on the variation of the displacement, moment and other response quantities. No mention has been made of how the stresses within the soil are distributed and how well this distribution is captured.

The stress distribution in the soil is related to gradients of the field quantity, and gradients in a given element depend on field quantities at nodes attached to that element. In general, adjacent elements display different states of stress at a node they share. Therefore, stress contours are actually discontinuous across inter-element boundaries. Large discontinuities indicate coarse discretization, while

almost continuous bands indicate unnecessarily fine discretization. However, typical FEM softwares average the nodal values calculated from the stress functions defined within the elements, hence providing a continuous stress contour across the model. Although the smoothed and averaged version of the stress contours is visually pleasing, it could be physically misleading. Therefore in the model developing and optimization stage, it is helpful to command the software to plot the discontinuous version of the stress plots in order to have an understanding of how well the model is constructed. It is desired to have this inter-element averaging of stress to a low value providing that the functions defined in neighboring elements terminating at a common node do not have a large difference in their values. The larger this difference is, less precise are the obtained results. This can be avoided by using an optimum number of elements to define the model. Therefore, checking the degree of discontinuity is a way to validate model optimization. To this end an invariant stress quantity; the Von Mises contours are presented in figures 1.25 and 1.26 for 100ft and 50ft shafts with 10, 20 and 40 longitudinal layers for 6 transverse layers. The vertical cross-section of the soil model is presented in these figures. The stresses are caused by the lateral movement of the shaft (not shown), which is inside the void space between the left and right soil cross section. Plot (a) in figure 1.25 shows the discontinuous Von-mises distribution in a 10-layer vertical and 6 layer lateral model. Plots (b) and (c) show the 20 and 40-layer versions respectively. Note how the maximum Von-mises stress changes from 1.185 ksf to 1.070ksf with an approximate 11% decrease, when the number of layers is changed from 10 to 20 and to 1.066 ksf when the number of layers is changed from 20 to 40. Also note the reduction in the discontinuity of stress

contours on an element-by-element basis as the number of layers is increased. Plot (d) is the averaged version of plot (c).

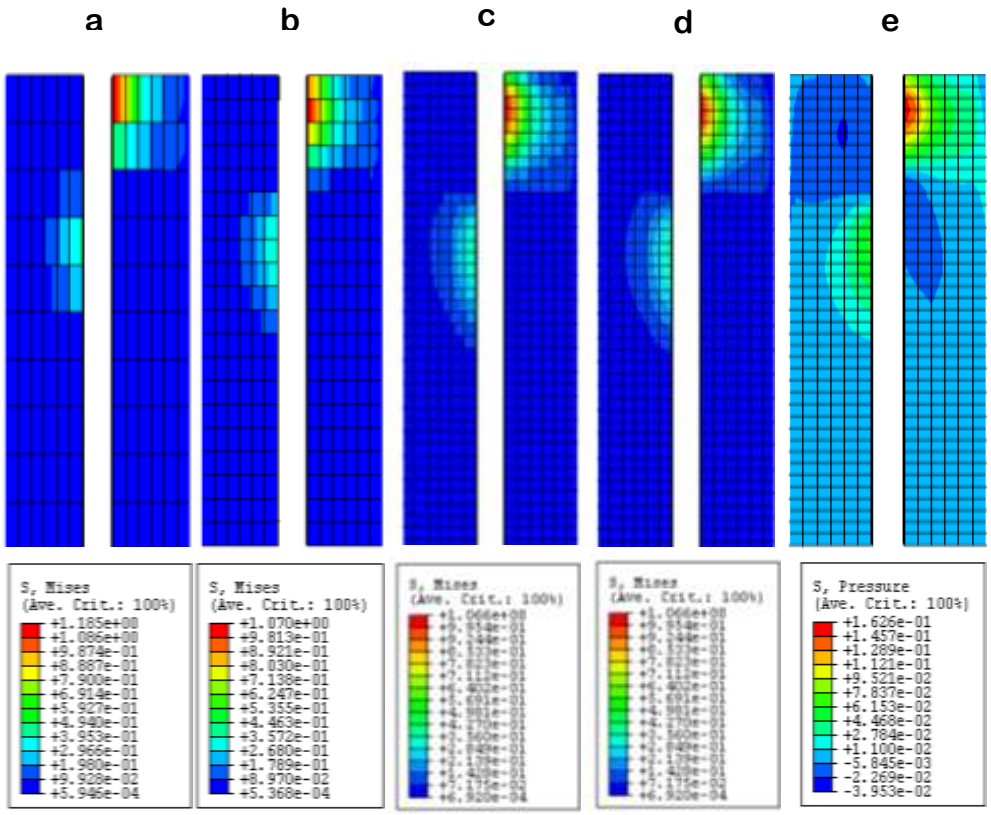

Figure 1.25 – Von mises and pressure contours for 100ft deep shaft

Plot (e) in figure 1.25 shows the pressure stresses within the soil. Note the positive pressure at the top-right and low-left part of the upper half of the model. The pressure profile gives us information about the movement of the shaft and the effective depth of the shaft that participates in resisting lateral loads. From this plot it is seen that the majority of the contribution to lateral loads comes from the top half of the shaft.

The figures and discussion above is repeated for 50ft shaft in figure 1.26.

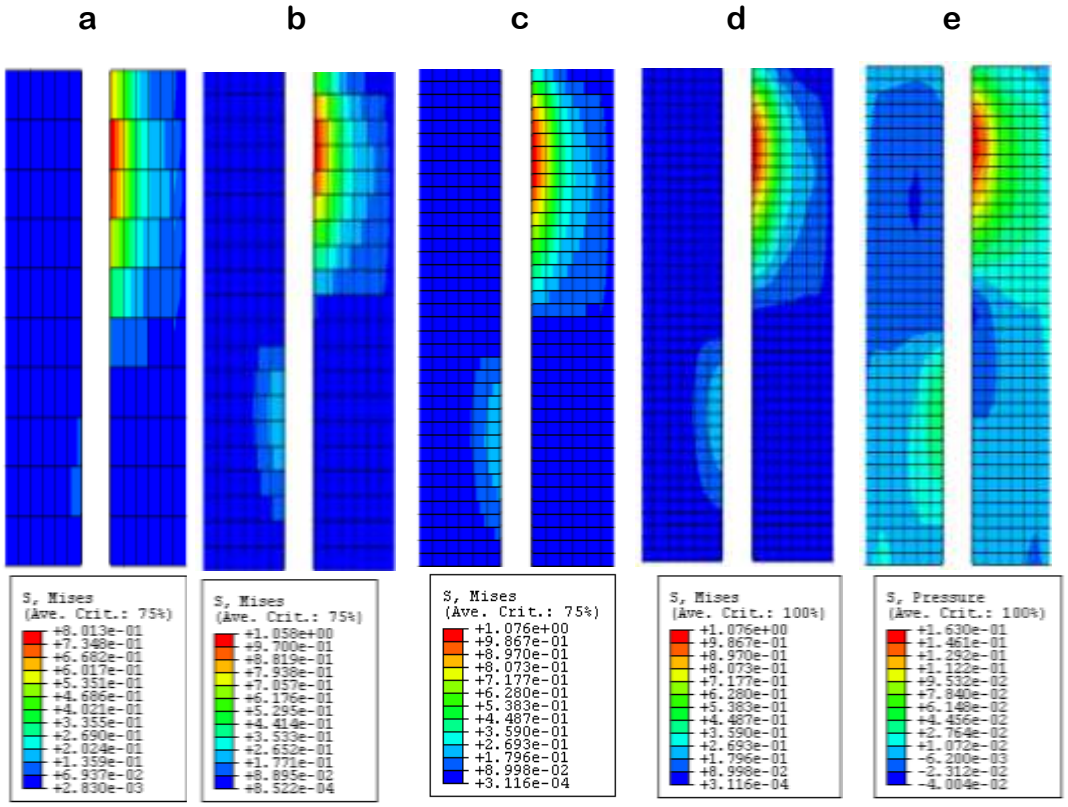

Figure 1.26 – Von mises and pressure contours with for 50ft deep shaft.

Note that unlike the slender case of 100ft deep shaft with 6 ft diameter, the case of the 50ft deep shaft with 6 ft diameter shows that, the portion of the shaft effective in resisting lateral load has extended almost the full length of the shaft.

The analysis of the deformation characteristics of the shaft as well as the stress distribution within the model led to the decision of using a FEM with element sizes 2.5% vertical size of the structure and a 4 element per quadrant distribution with soil extension of 2.5D divided in 5 layers. The proposed model for Type-1 FEM is shown in figure 3.27. Total number of d.o.f is 20793 and the total number of elements is 5696, of which 640 are CIN3D8 elements, 3856 are C3D8 elements and 1200 are C3D8R elements. The average analysis time on a 2.4Ghz PC was 10 minutes. Figure 1.28 shows displaced shape of a laterally loaded 100ft shaft.

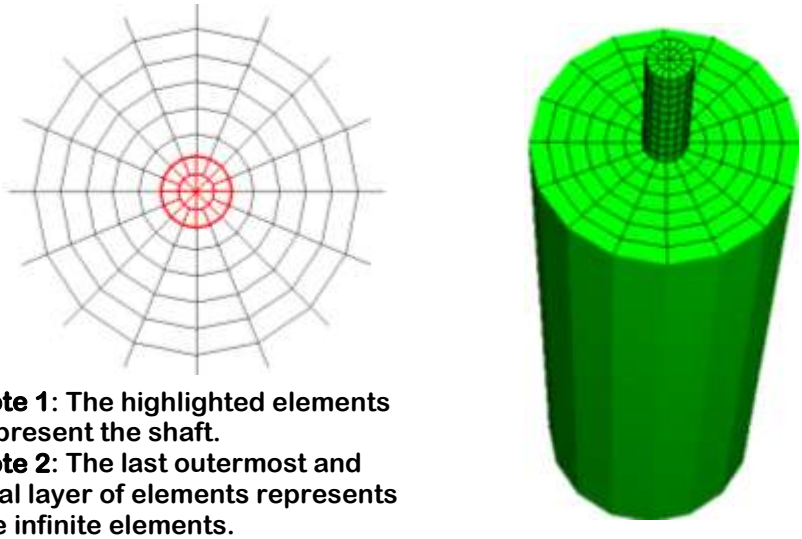

Note 1: The highlighted elements represent the shaft.
Note 2: The last outermost and final layer of elements represents the infinite elements.

Figure 1.27 – FEM for SSI model Type-1

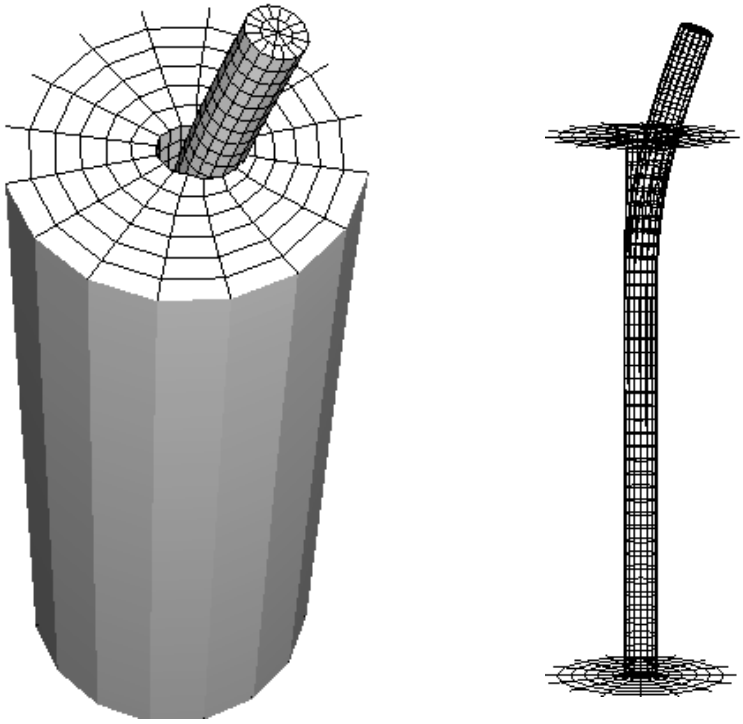

Figure 1.28 – Perspective and elevation view of a Type-1 laterally loaded shaft.

1.2.2.2.3.2 SSI Modeling Including Soil Selfweight

In this FE model, the soil selfweight was included and the soil domain within the SSI model had to be extended (Type-2 FEM). The reason for this extension was the amount of soil around the shaft that contributed to confinement of the drilled shaft reached a wider zone than the Type-1 model. When the soil weight was included, the effective soil volume around the shaft had more influence on the shaft response compared to the case with no soil selfweight. The effective soil mass was approximated through the depth of the soil layer and the friction angle of the soil as proposed in section 1.1.1.2. In the Type-2 FEM, single soil layer i.e. dense dry sand extends the whole depth of the shaft. To this end, in order to see the contributing soil mass around the drilled shaft, various models with different soil extensions were analyzed in order to validate the assumed extension. The soil was extended from 1D to 10D away from the shaft surface and the resulting displacements and moments were recorded. Once the point of convergence was established, the amount of element layers within this optimum distance were decided through a series of models that included element layers ranging from 5 to 10. From figures 1.29 (a), (b) and (c) it is seen that the parameters of interest converge to a boundary value at a soil extension of about 8D from the shaft surface compared to 2.5D when the selfweight was not included. The above results showed that the variation of results beyond 6D were minimal. The rate of change of the results obtained from an extension of 6D to 8D is very small and extending the soil layer beyond 8D does not change the confinement effects on the shaft.

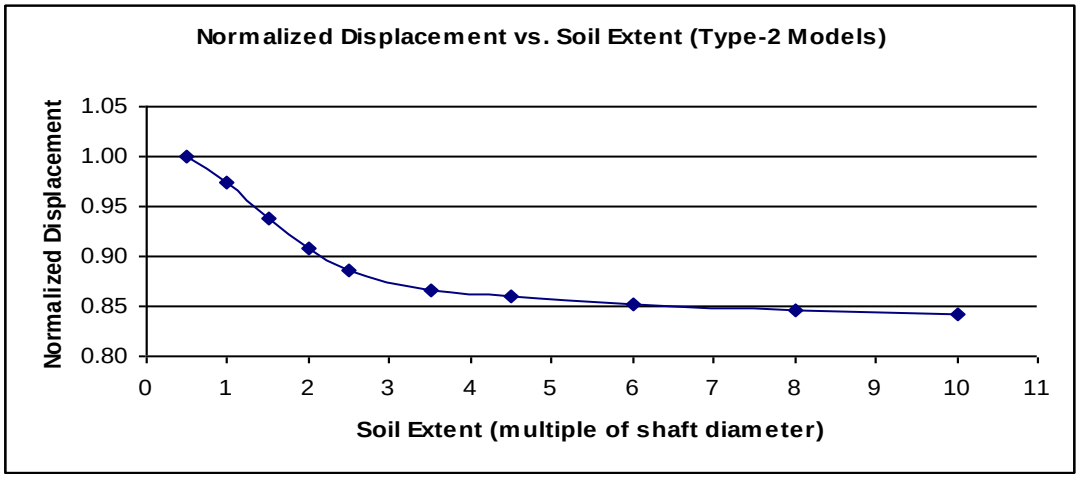

(a) Maximum displacements normalized with respect to 0.5D soil extension.

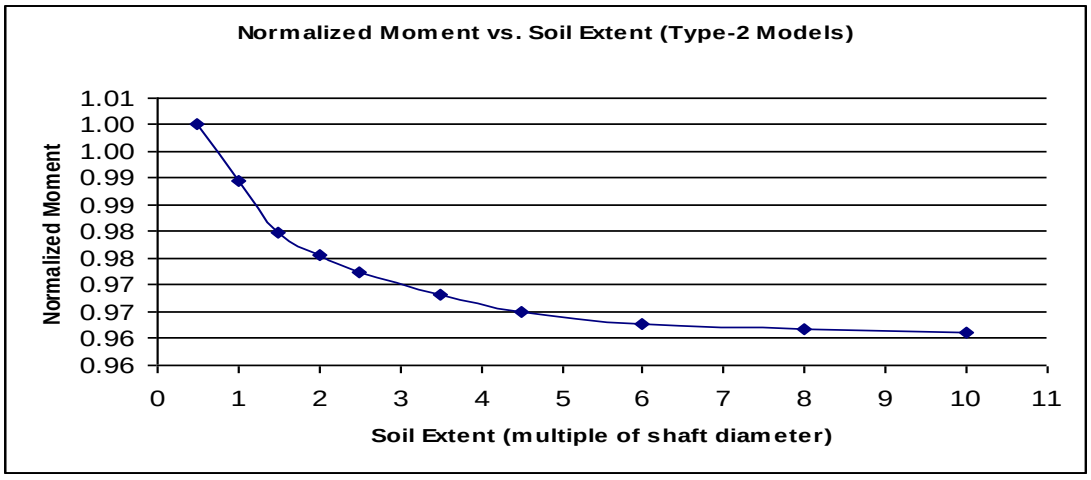

(b) Maximum moment normalized with respect to 0.5D soil extension.

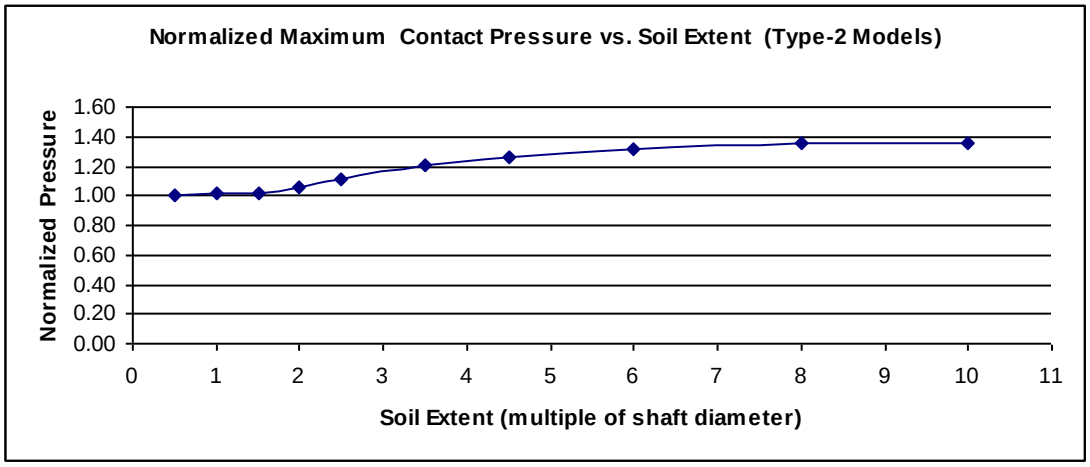

(c) Maximum pressure normalized with respect to 0.5D soil extension

Figure 1.29 –Variation of maximum response parameters with soil volume.

For the shaft dimensions analyzed; 6D equals a distance of 36 ft and 8D equals a distance of 48 ft. According to the proposed equation in section 1.1.1.2 the effective extension turns out to be E=L.cos(45°+36°/2)=45.4ft where ϕ=36°. The result obtained from this equation is approximately 7.5D. Thus the results obtained from the FEM are in agreement with the expected value from equation (2) in section 1.1.1.2. An 8D soil extension was selected for the models used in this study.

Once the extension was set, the soil mesh was determined. The number of elements used within this extension varied and the displacements were obtained under the same loading conditions. Figure 1.30 shows the effect of the radial distribution of elements for the 8D soil extension. Although the differences did not vary significantly as in the case for for Type-1 FEM, the increase in the number of elements from 5 to 11 within the soil effective zone resulted in a 3% difference change in displacement. This increase is due to the use of more finite elements within that distance.

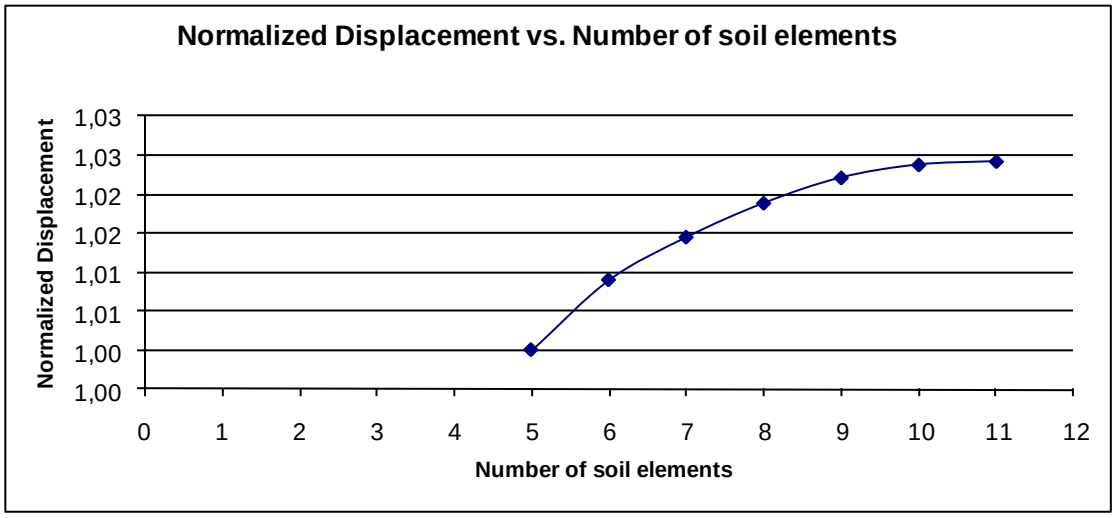

Figure 1.30 – Percentage increase in displacements with increasing number of layers.

The decision made for selecting the soil effective zone and mesh size was not based on the displacements and moments alone. A study of discontinuous stress contours was also conducted as well. Figure 1.31 shows the discontinuous stress distribution among the soil elements under the self-weight of the soil. The argument for Type-1 FEM also applies for the Type-2 FEM. An increase in the number of element in the transverse direction reduces the discontinuities of the element-based stresses. Also the change in maximum Von-mises stress value from 5.528ksf to 6.212 ksf resulted in an approximate 11% increase. The use of element size approximately 10% of the soil extension was shown to be sufficient.

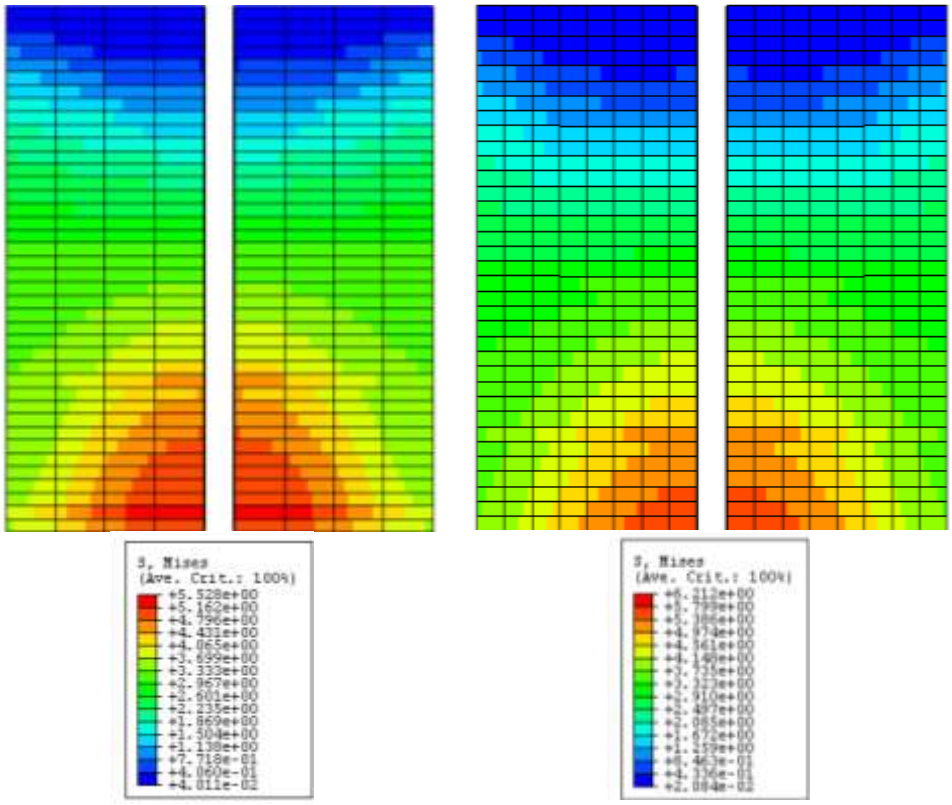

Figure 1.31 – Von mises stresses in 4 and 8 layer meshes

Based on these results it was decided that the effective soil extension is a function of the stability criteria of the soil, which is case dependent. The inclination of the failure plane, which is dependent on the internal friction angle of the soil and the soil layer depth are the main factors that determine the extent of soil in the FEM. In cases where there were multiple layers of soil along the depth of the shaft, the combination of individual layer depth and individual friction angle that gives the maximum soil extension should be used. In the model analyzed in this section, only one single soil layer was used that extended the whole depth of the shaft. Thus the effective soil mass around the shaft is related to the depth of the shaft and the friction angle. Figure 1.32 shows the model for Type-2 SSI model with 8D extension and 8 divisions. This model was used in this study when the selfweight was included. The total number of d.o.f is 24681 and the total number of elements is 6960, of which 640 are CIN3D8 elements, 5120 are C3D8 elements and 1200 are C3D8R elements. The average analysis time on a 2.4Ghz PC is 12 minutes.

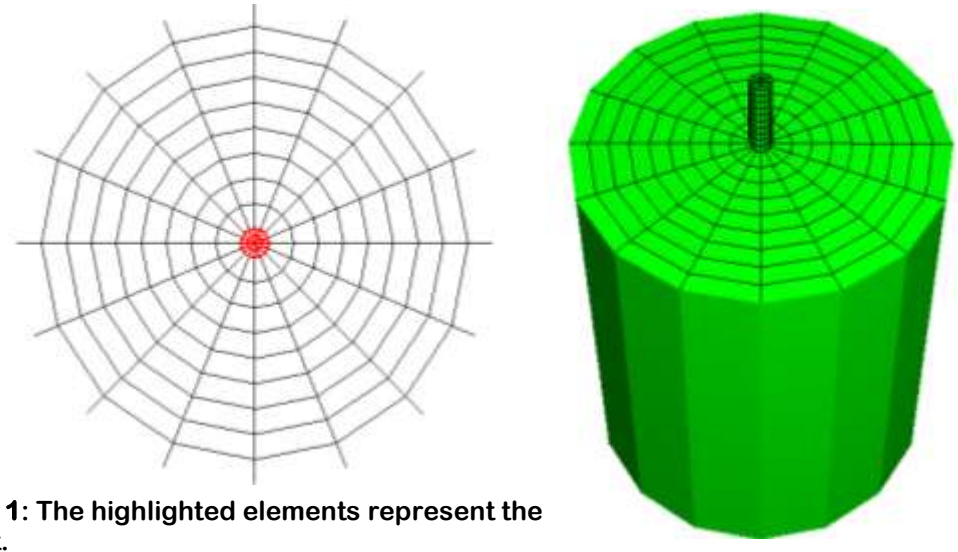

Note 1: The highlighted elements represent the shaft.

Note 2: The outer layer represents the infinite

Figure 1.32 – FEM for SSI model (Type-2)

Figure 1.33 shows the soil displacements due to selfweight and the shaft displacement due to lateral load. The loading sequence in the analysis was divided into 2 steps: (1) soil deformations followed by, (2) lateral loading on the shaft.

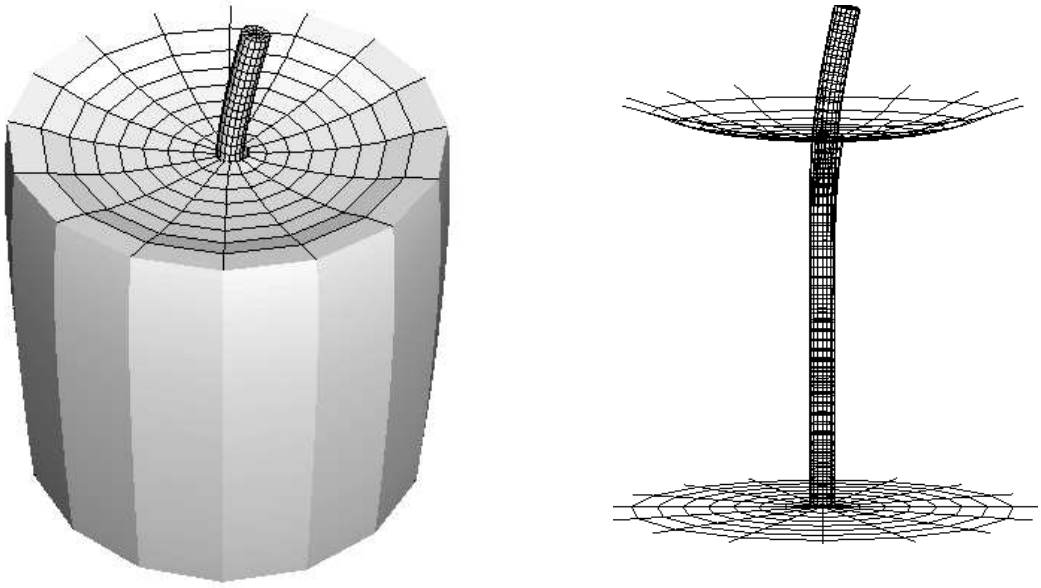

Figure 1.33 – Perspective and elevation view of a Type-2 laterally loaded shaft.

REFERENCES

1. ABAQUS Standard/Explicit Manuals versions 6.3&6.4

2. Anderson, Townsend. (2002) “A Laterally Loaded Pile Database”. Deep Foundations 2002: An International Perspective on Theory, Design, Construction, and Performance pp. 262-273

3. Baker (1993). “Use of Pressuremeter in Mixed Highrise Foundation Design”. Design and Performance of Deep Foundations: Piles and Piers in Soil and Soft Rock pp. 1-13

4. Boulanger, Hutchinson, Chai, Idriss (2004). "Estimating Inelastic Displacements for Design: Extended Pile-Shaft-Supported Bridge Structures” Earthquake Spectra, Vol. 20, No. 4, pp. 1081-1094.

5. Bowles (1997). “Foundation Analysis and Design 5th Edition” MacGraw-Hill Companies

6. Briaud, Buchanan (2000) “Introduction to Soil Moduli”.

7. Briaud, L.L., Smith, T.D. Tucker, L. (1985). "Pressuremeter Design Method for Laterally Loaded Piles," Proceedings of the XI International Conference on Soil Mechanics and Foundation Engineering, San Francisco, CA, U.S.A.,

8. Briaud, Johnson, Stroman (1984). “Lateral Load Test of an Aged Drilled Shaft” Laterally loaded deep foundations: Analysis and performance, STP 835 pp. 172-181

9. Britto, Gunn, (1987) Critical State Soil Mechanics Via Finite Elements Ellis Horwood Limited

10. Chen, Liu (1990). “Development in Geotechnical Engineering 52 -Limit Analysis and soil plasticity” -Elsevier Publishing

11. Chen, Mizuno (1990) “Developments in geotechnical engineering53 -Nonlinear Analysis in Soil Mechanics Theory and Implementation”- Elsevier Publishing

12. Chen (1975) “Development in Geotechnical Engineering 7 -Limit Analysis and soil plasticity”- Elsevier Publishing

13. Choi, Oh, Kwon, Kim. (2002) “A Numerical Analysis for Axial and Lateral Behavior of Instrumented Steel Pipe Piles”. Deep Foundations 2002: An International Perspective on Theory, Design, Construction, and Performance pp. 289-304

14. Cook, Malkus, Plesha, Witt (2002). "Concepts and Applications of Finite Element Analysis 4th Edition" John Wiley and Sons Inc.

15. Dameron, Arzoumanidis, Bennett, Malik (1999). "Seismic Analysis and Displacement Based Evaluation of the Brooklyn-Queens Expressway".

16. Das (1999) "Principles of Foundation Engineering 4th edition" PWS Publishing

17. Dessai, Abel (2002). "Introduction to Finite Element Modeling". CBS Publishers & Distributers

18. Duggal, Bohinsky, Chu. (1989) "Comparative Performance of Two Pile Types" Foundation Engineering, pp. 943-956

19. Habigaghi, K. and Langer, J.A. (1984). "Horizontal Subgrade Modulus of Granular Soils". Laterally loaded deep foundations: Analysis and performance, STP 835 pp. 21-34

20. Horvath, (1984). "Simplified Elastic Continuum Applied to the Laterally Loaded Pile Problem". Laterally loaded deep foundations: Analysis and performance, Laterally loaded deep foundations: Analysis and performance, STP 835 pp. 229-238

21. Horvath J.S. (2002) "Soil-Structure Interaction Research Project:Basic SSI Concepts and Applications Overview" Report No. CGT-2002-2

22. Huang, Ye, Tang. (2002) "Dynamic Coupled Analysis for Earthquake Response of Pile Foundations". Deep Foundations 2002: An International Perspective on Theory, Design, Construction, and Performance pp. 396-404

23. Kappos, Sextos (1999) "Effect of Foundation Type and Compliance on Seismic Response on RC Bridges". Journal of bridge engineering, Vol.6, No.2, March 2001.

24. Kulhawy. (2002) "Observations on Some Shortcomings in Foundation Analysis and Design". Deep Foundations 2002 (GSP 116), pp.1-5.

25. Kulhawy, Cushing.(2002) "Drained Elastic Behavior of Drilled Shafts in Cohesionless Soils". Deep Foundations 2002: An International Perspective on Theory, Design, Construction pp. 22-36

26. Kulhawy, Agaiby, Trautmann (1996) "On large scale model testing of laterally loaded drilled shafts in sand " Geotechnical Testing Journal , vol.v19., no.n1., pp.pp32-40.

27. Kulhawy, F. H. (1991). "Drilled shaft foundations , Foundation engineering handbook".

28. Kumar, Kort, Hosin, and Chong (2004) “Lateral Load Tests on Small Diameter Drilled Piers”

29. Kumar, Alizadeh (2002). “Lateral Load-Deflection Response of Single Piles in Sand”.

30. Kort, Kumar, Hosin, Ng (2002) “Lateral Load Tests on Small Diameter Drilled Piers”.

31. Lin,Yang, Juang, Lee (2000). “Analysis of Laterally Loaded Piles in a Two-Layered Elastic Medium”.

32. Lee, Kane, Bennett, Drumm (1989) “Investigation and Modeling of Soil-Structure Interface Properties”

33. Lee (1991) “Discrete Layer Analysis of Laterally Loaded Piles”.

34. Long, Reese (1984). “Testing and Analysis of Two Offshore Drilled Shafts Subjected to Lateral Loads”. Laterally loaded deep foundations: Analysis and performance, STP 835 pp. 215-228

35. Luna, Jadi (1998) “Determination of Dynamic Soil Properties Using Geophysical Methods”.

36. Macklin, Nelson, Chou (1993) “A Lateral Load Test on Seven Foot Diameter Caissons”.

37. Maharaj (1997)“Load-Deflection Response of Laterally LoadedSingle Pile by Nonlinear Finite Element Analysis”.

38. Matlock, Reese, (1960). Generalized Solutions for laterally Loaded Piles, Journal of the Soil Mechanics and Foundations Division, ASCE, Vol.86, No SM5, Proc.Paper 2626, pp.63-91

39. Motan, Gabr. (1989) “A Flat-Dilatometer Study of Lateral Soil Response.”

40. Neate (1983) “Augered Cast in Place Piles”.

41. Neely (1979) “Bearing pressure-SPT Correlations for Expanded Base Piles in Sand”.

42. Olson, Clifford, Wright (1983) “Nondestructive Testing of Deep Foundation with Sonic Methods”.

43. Petek, Felice, Holtz. “Capacity Analysis of Drilled Shafts with Defects”.

44. Pise, P. J. (1983), Lateral Response of Free-Head Pile, Journal of Geotechnical Engineering, ASCE, Vol. 109, No.8 pp. 1126-1131.

45. Popov (1998) “Engineering Mechanics of Solids 2nd Edition” Prentice Hall Publishing.

46. Prakash, Sharma (1990) “Pile Foundations in Engineering Practice”. John Wiley and Sons Inc.

47. Puppala, Moalim (1986) “Evaluation of Driven Pile Load Capacity Using CPT Based LCPC and European Interpretation Methods”.

48. Pyle, R. and Beikae, M. (1984). “A New Solution for the Resistance of Single Piles to Lateral Loading” Laterally Loaded Deep Foundations: Analysis and Performance, STP 835 835 pp. 3-20

49. Reese, Wright, Aurora (1984). “Analysis of a Pile Group Under Lateral Loading”. Laterally loaded deep foundations: Analysis and performance, STP 835 pp. 56-71

50. Reese, L.C., and Matlock, H., (1956). “Non-Dimensional Solutions for Laterally Loaded Piles with Soil Modulus Assumed Proportional to Depth”, Proceedings, Eighth Texas Conference on Soil Mechanics and Foundation Engineering,

51. Roberston, Hughes (1984). “Design of Laterally Loaded Displacement Piles Using a Driven Pressuremeter”. Laterally loaded deep foundations: Analysis and performance, STP 835 pp. 229-238

52. Sogge (1984). “Microcomputer Analysis of Laterally Loaded Piles”. Laterally Loaded Deep Foundations: Analysis and Performance, STP 835 pp. 35-48.

53. Smith, T.D., (1989) "Fact or Friction: A Review of Soil Response to a Laterally Moving Pile", Proceedings of the Foundation Engineering Congress, Northwestern University, Evanston, Illinois, pp. 588-598

54. Smith, T.D., Slyh, R. (1986) "Side Friction Mobilization Rates for Laterally Loaded Piles from the Pressuremeter, “ Proceedings of the Second International Symposium, The Pressuremeter and its Marine Application”, Texas A&M, May ASTM STP 950, pp. 478-491

55. Taciroglu, Rha, Stewart, Wallace, (1999). “Robust Numerical Models for Cyclic Response of Columns Embedded in Soil”.

56. Vennalaganti, Endley, Rao (1992) “Lateral Loads on Long piles and piers in granular soils”.

57. Wang, Rinne (1999) “Pile Foundation Construction Practice in Stiff Clays with Dense Granular Layers”.

58. Woodward, Gardner, Greer. (1972) “Drilled Pier Foundations” McGraw Hill Publishing

59. **Zhang, Tulla, Grismala (1977) "Ultimate Resistance of Laterally Loaded Piles in Cohesionless Soils".**

60. **Zafir (1986) "Seismic Foundation Stiffness for Bridges".**